A Generalized Two-Dimensional FFT Precoded Filter Bank Scheme With Low Complexity Equalizers in Time-Frequency Domain

Rogério Pereira Junior, Carlos Aurélio Faria da Rocha, Bruno Chang, Didier Le Ruyet

Digital Object Identifier

A Generalized Two-Dimensional FFT Precoded Filter Bank Scheme with Low Complexity Equalizers in Time-Frequency Domain

ROGÉRIO PEREIRA JUNIOR[1], CARLOS A. F. DA ROCHA[2], BRUNO S. CHANG[3] AND DIDIER LE RUYET[4],

[1]Federal Institute of Santa Catarina, São José, Brazil (e-mail: rogerio.pereira@ifsc.edu.br)
[2]Federal University of Santa Catarina, Florianópolis, Brazil (e-mail: carlos.aurelio@ufsc.br)
[3]CPGEI/Electronics Department, Federal University of Technology - Paraná, Curitiba, Brazil (e-mail:bschang@utfpr.edu.br)
[4]CEDRIC, Conservatoire National des Arts et Métiers, Paris, France (e-mail:leruyet@cnam.fr)

Corresponding author: Rogério Pereira Junior (e-mail: rogerio.pereira@ifsc.edu.br).

ABSTRACT Recently, the two-dimensional (2D) fast Fourier transform (2D-FFT) filter bank (FB) technique was proposed as an alternative to new wireless communication technologies covering several application scenarios. This technique presents similar characteristics to orthogonal time-frequency space modulation (OTFS), such as lower PAPR and robustness in high mobility scenarios; in addition, thanks to the use of filter bank modulation, the technique has a good spectral localization. In this work, we present the generalization of the 2D-FFT FB system by making changes in the waveform structure to obtain advantages in the symbol detection process. The proposed idea allows the use of low-complexity equalizers in the time-frequency (TF) domain, bringing a good performance/complexity trade-off and obtaining bit error rate (BER) results of the same order than delay-Doppler domain receivers for OTFS. Theoretical and simulation results show that it is possible to obtain a good error performance in high mobility scenarios even using simple equalizers in the TF domain combined with waveform structure adjustments.

INDEX TERMS 2D-FFT, Filter Bank, High Mobility, Rate Factor, Time-Frequency Domain

I. INTRODUCTION

Orthogonal frequency division multiplexing (OFDM) is the most used multi-carrier technique in modern communication systems, due to its robustness against dispersive channels. Its applications stand out in fourth and fifth generation (5G) wireless communication systems, the focus of much study and research up to now due to its applicability in various sectors of the industry. For these systems, features such as low latency, energy efficiency, robustness in high mobility scenarios and support for thousands of devices are essential to meet and expand the requirements of different use cases. In addition, the available electromagnetic spectrum is increasingly restricted, so that studies of future wireless systems in millimeter waves and with better spectral confinement are also important and current research topics [1]. Thus, future networks such as sixth generation (6G) mobile systems must be able to expand and meet this demand, introducing new forms of efficient transmission. In this sense, the OFDM technique does not meet all of these requirements. The lack of robustness over time-varying communication channels with high Doppler propagation, high peak to average power ratio (PAPR) and the problem with out-of-band (OOB) emissions require changes in the OFDM transmission structure, such as additional filtering to meet metrics imposed by modern wireless systems.

The filter bank multi-carrier (FBMC) system is an alternative to mitigate the high OOB emissions inherent to OFDM [2]. This technique is based on subcarrier filtering and does not use a guard interval (increasing the spectral efficiency) in order to improve the spectral location and consequently to limit the OOB emissions [3]. However, the filtering process generates interference on the imaginary coefficients and consequently the loss of complex orthogonality of the system. Thus, it is necessary to relax the complex orthogonality criterion to the real field, motivating the use of offset quadrature amplitude modulation (OQAM) [4]. Through OQAM, the

imaginary and the real part are transmitted separately with a shift of half of the symbol period between them. On the receiver side, the data is transported only by the real (or imaginary) component, while the intrinsic interference term appears in the imaginary (or real) part [2]. Thus, a transmission of only real symbols is generated at a double rate (to maintain maximum transmission capacity) free from filter interference. However, even though the interference is orthogonal to the data symbols, the loss of complex orthogonality prevents combining FBMC with some multiple input/output (MIMO) techniques, such as space-time block coding and spatial multiplexing (SM) with maximum likelihood (ML) detection [5]. In short, the FBMC system solves spectral localization problems using the restricted available spectrum more efficiently; however, problems arise for application in MIMO systems, in addition to maintaining the problems of high PAPR and Doppler sensitivity as OFDM.

In FBMC systems, the interference from the filter bank must be eliminated to recover complex orthogonality. The use of discrete Fourier transform (DFT) as a way of spreading the data either in the time or frequency domain can be used for this purpose. In [5] time spreading via inverse-DFT (IDFT) was proposed in order to recover the complex orthogonality. Using an OFDM-based precoding, the authors aim to isolate and eliminate the intrinsic interference of the filter. In the same segment, the authors in [6] presented the Pruned DFT-spread FBMC, which is based on frequency spreading combined with a filter compensation stage. Compared to the single-carrier frequency-division multiple access (SC-FDMA) system, the system proposed in [6] has many similarities. The differences consist in the addition of a filter compensation stage and changing the core of the system from an OFDM modulator to an FBMC one transmitting at double rate. For this reason, the system presents the main advantages of SC-FDMA and FBMC, such as low PAPR, better spectral confinement, and a certain robustness to Doppler spreading. In [7], we presented the DFT precoded filter bank system. This scheme also uses the double rate transmission principle and is similar to the Pruned DFT one, but avoids the use of OQAM through a new transmission strategy, reducing complexity and making it possible to add flexibility to the filter bank structure. This flexibility had been initially explored in [8] where another type of precoding was used. However, the objective was to study the impact on the rejection of interference coming exclusively from the filter, since the precoding technique applied was based on the spreading of the symbols in time. In this sense, taking advantage of the symbol spreading characteristics in the frequency domain of [7], we proposed in [9] a generalized DFT precoded filter bank system. Unlike the FBMC/OQAM system and its precoded versions mentioned so far, which operate according to the double rate principle, in the proposed system this is modified so that transmissions via filter bank can be done differently. The technique has, as advantages over other systems, lower PAPR and better performance in high mobility scenarios. Finally, in [10] we also proposed the use of a two-dimensional (2D) DFT as precoding for the FBMC system, which is similar to the approach taken in the time-frequency space modulation (OTFS) technique. It is known that for the technique to work, complex orthogonality between the base pulses is necessary, which is not present in conventional FBMC. However, as previously reported, with the use of precoding via DFT it is possible to recover this orthogonality. Thus, the system proposed in [10] called Two-Dimensional FFT filter bank (2D-FFT FB) uses a part of the coding performed in OTFS in order to recover this orthogonality. In this sense, the filter bank can be used so that the technique obtains the main advantages of the FBMC and OTFS [11] systems. In OTFS system, information symbols are placed on a so-called delay-Doppler (DD) grid, mapped to symbols on a time-frequency (TF) grid by a two-dimensional DFT and transmitted over the channel using the multi-carrier OFDM technique [12]. In our proposed technique, the same mapping is performed, however the symbols are transmitted using a filterbank at double rate. Using the data transmission strategy and the coding performed by the two-dimensional DFT, the complex orthogonality is recovered. Furthermore, good error performance is obtained in high mobility scenarios with only a simple equalizer in the TF domain, a feature that will be better explored in this work.

Based on the results obtained in [9] and [10], a generalized 2D-FFT FB scheme system is proposed in this work. The waveform of the filter bank is modified using the rate factor parameter, and the combination of this new technique with low-complexity time-frequency equalizers is explored. The main idea is to show that it is possible to obtain similar performance, using these TF equalizers, as the one obtained with more complex OTFS receivers working in the delay-Doppler domain. In addition, a significant PAPR reduction is also obtained using this generalized system, as it will be shown in the sequel. In short, the main contributions of this work are:

1) Generalization of the filter bank structure through a rate factor, providing greater robustness in certain application scenarios.
2) Analysis of the impact of this generalization in terms of PAPR and error performance via the signal-noise-plus-interference ratio (SINR), the signal-interference ratio (SIR).
3) Analysis of a low-complexity receiver in the time-frequency domain with good performance.

The remainder of this article is organized as follows: Section II describes the generalized 2D-FFT filter bank system with the rate factor parameter, as well as the process of restoring complex orthogonality via precoding of this system. Section III presents the derivation of equalizers in the TF domain to be compared with receivers studied in OTFS. Section IV presents the analysis of performance in doubly selective channels deriving the SIR and SINR equations. Simulation results, comparisons, and a complexity study are presented in Section V. Finally, Section VI concludes the

article and presents some future perspectives.

Notation: vectors and matrices are represented by lowercase and uppercase letters in bold, respectively. The superscripts $(.)^T$ and $(.)^H$ denote, respectively, transpose and Hermitian transpose operations. The identity matrix of size $N \times N$ is denoted by $\mathbf{I}_N$. We will use $[\mathbf{M}]_{i,j}$ to refer to the $(i;j)$-th element of a matrix $\mathbf{M}$, and $[\mathbf{m}]_i$ to i-th element of the vector $\mathbf{m}$. The diag($\mathbf{M}$) produces a new vector with the same elements as the main diagonal of $\mathbf{M}$ and diag($\mathbf{m}$) represents the generation of a diagonal matrix of the elements of the vector $\mathbf{m}$. The column vectorization of a matrix is represented by vec(.). The term (x mod y) means the remainder of dividing x by y, and therefore is always a value between 0 and $(y-1)$.

II. GENERALIZED 2D-FFT FILTER BANK SYSTEM

A. BACKGROUND

It is possible to restore the complex orthogonality in FBMC schemes with precoding techniques [13] and, according to the system arrangement, to avoid the use of the OQAM modulation. In this sense, it is possible to work with different transmission rates from the conventional double-rate FBMC/OQAM systems, making the waveform structure more flexible. To begin, let us denote by $x_{l,k}$ a transmitted symbol at the l-th subcarrier at the k-th index time of a multicarrier system. Thus, a baseband signal transmitted by a filter bank can be written as

$$s[m] = \sum_{l=0}^{L-1} \sum_{k=0}^{K-1} x_{l,k} g_{l,k}[m], \tag{1}$$

where m represents the m-th discrete time instant and $g_{l,k}[m]$ is given by

$$g_{l,k}[m] = g[m - kL/2] e^{j\frac{2\pi l}{L}(m - kL/2)}. \tag{2}$$

which is essentially a time and frequency-shifted version of the prototype filter $g[m]$, while K indicates the number of multi-carrier symbols in time domain with L subcarriers each. The pulse used in the filtering process has unity energy and its length is given by OL, where O is generally referred to as the overlap factor that controls the duration of the pulse. We assume that the prototype filter $g[m]$ is zero outside the time interval $0 \leq m \leq OL-1$. According to the Balian-Low theorem [14], base functions with complex orthogonality have necessary infinite dispersion in time or in frequency. The use of a filter well located in time and frequency restricts this characteristic; thus, other properties imposed in the theorem must be sacrificed for the waveform design. A resolution of this problem is well known for the SISO case by using OQAM modulation, where we transmit the real or imaginary part of a quadrature amplitude modulation (QAM) symbol every $L/2$ samples (half of a symbol period) as described by the equation (2). However, orthogonality between pulses is only obtained in the real field, which is a problem for MIMO scenarios and channel estimation.

The recovery of complex orthogonality can be done using precoding based on spreading in the time or frequency domain of the data symbols. In [6] and [7] a precoding scheme is proposed based on the frequency spreading via DFT, combined with a filter compensation stage to partially recover the complex orthogonality. Particularly, in [7] the authors propose the DFT precoded filter bank system where a strategy for allocating the transmitted data eliminates the need to use OQAM modulation and, consequently, does not require a phase shift between the symbols that are transmitted every $L/2$ samples. Basically from the defined L subcarriers, complex data symbols are transmitted at double rate on $L/2$ subcarriers. Such symbols are fed into the first and last $L/4$ bins of the L-point DFT. In this way the symbols that belonged to only one point in frequency, are now spread over all frequencies. With this transmission strategy, it is now possible to modify the time configuration of the transmitted signal, making waveform design more flexible [9]. Thus, we can generalize the structure of the filter bank by rewriting (2) as follows:

$$g_{l,k}[m] = g[m - kL/\beta] e^{j\frac{2\pi l}{L}(m - kL/\beta)}. \tag{3}$$

The term β is the rate factor and determines the interval of samples in which the transmission of symbols is performed. Necessarily, β needs to be a power of two. For example, (3) can represent a transmission of the symbols $x_{l,k}$ by an OFDM modulator if $\beta = 1$ and $g_{l,k}[m]$ is a rectangular filter with $O = 1$. In this case, symbols are transmitted every L samples. For the case where the filter prototype is not a longer rectangular window, the interference is generated due to the superposition of the pulses. This fact generates the loss of complex orthogonality between the pulses, requiring precoding techniques. With this generalization, now L/β complex symbols are allocated in the first and last $L/2\beta$ positions of an L-point DFT. Such generalization by the rate factor β presents robustness in high mobility scenarios in view of the shorter duration of the pulses. Considering an OFDM symbol of L subcarriers as a reference, each symbol in the generalization of the filter bank is composed by L/β complex symbols plus $L((\beta-1)/\beta)$ zeros. These symbols are spread in the frequency domain through an L-point DFT and transmitted using a rate factor equal to β, to obtain the same transmission rate as in OFDM. Figure 1 shows OFDM, FBMC/OQAM symbols and DFT precoded filter bank system with $\beta = 4$ and $L = 8$. Of course, to maintain the same density of transmitted symbols, FBMC/OQAM operates with a rate $T/2$, while in our system the symbols are sent at a rate T/β. In other words, to maintain the same symbol transmission rate the conventional FBMC system, for example, doubles the network/block density in time (K) in relation to OFDM when adopting OQAM. The idea in this work is to adapt this generalization strategy to the 2D-FFT FB system [10], due to its greater robustness in these scenarios and the good performance of the one-tap frequency domain equalizer compared to the OTFS system.

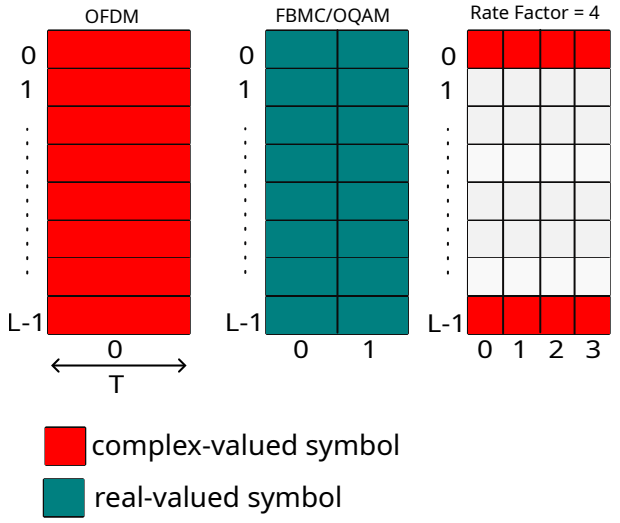

Figure 1: Data transmission structure for OFDM, FBMC/OQAM and DFT precoded systems to $L = 8$.

B. SYSTEM MODEL

In the proposed system, data symbols are spread in both time and frequency domains using the Inverse Symplectic Finite Fourier Transform (ISFFT), a two-dimensional discrete Fourier transform. Figure 2 shows the block diagram of the proposed system and the principle of this scheme can be summarized as follows.

Initially, LK/β information symbols coming from a QAM constellation are mapped into a delay-Doppler grid whose information in the m-th delay index of the n-th Doppler index is represented by $a_{m,n}$. The information symbols are inserted in the first and last $L/2\beta$ positions in the delay domain and the remaining positions are filled with zeros. For a fixed Doppler index n, we can represent this mapping in the vector $\mathbf{a}_n$ as follows

$$\mathbf{a}_n = [a_{0,n}\ a_{1,n}\ \dots\ a_{\frac{L}{2\beta},n}\ 0\ \dots\ 0\ a_{L-\frac{L}{2\beta},n}\ \dots\ a_{L-1,n}]^T. \quad (4)$$

Thus, denoting the subcarrier spacing in the frequency domain by F, we have a delay-Doppler grid with L points along the delay dimension with spacing $\Delta\tau = \frac{1}{LF}$, and K points along the Doppler dimension with spacing $\Delta\nu = \frac{1}{KT/\beta}$. Its representation can be expressed by

$$\mathbf{\Gamma} = \left\{ \left(\frac{m}{LF}, \frac{n}{KT/\beta} \right),\ m = 0, \dots, L-1; n = 0, \dots, K-1 \right\}. \quad (5)$$

Consequently, the transmission bandwidth B is the inverse of the delay resolution and the total transmission duration KT is the inverse of the Doppler resolution. To apply the ISFFT, first the symbols $a_{m,n}$ pass through a K-point IDFT, yielding $\bar{a}_{m,k}$ which is given by

$$\bar{a}_{m,k} = \sum_{n=0}^{K-1} a_{m,n} e^{j\frac{2\pi kn}{K}}. \quad (6)$$

Then, with the established transmission strategy, the complex orthogonality restoration process is complemented with a filter compensation factor and frequency spreading via L-points DFT. Thus, the output signal $x_{l,k}$ of the codification process can be written as

$$x_{l,k} = \sum_{m=0}^{L-1} \bar{a}_{m,k} b_m e^{-j\frac{2\pi ml}{L}}, \quad (7)$$

where b_m is the filter compensation coefficient. Replacing (6) into (7) the output signal $x_{l,k}$ can be expressed by

$$x_{l,k} = \sum_{m=0}^{L-1} \sum_{n=0}^{K-1} a_{m,n} b_m e^{j2\pi(\frac{nk}{K} - \frac{ml}{L})}. \quad (8)$$

From (8) we can see that we have applied an ISFFT to the data symbols, which is similar to the OTFS technique. Thus, through the ISFFT, the information symbols $a_{m,n}$ in the DD domain are mapped onto complex symbols $x_{l,k}$ in the time-frequency domain. The time-frequency grid consists of L points along the frequency domain with spacing F and K points over the time domain with spacing T/β. Figure 3 presents this mapping done by the ISFFT. Note that in the delay-Doppler domain L represents the number of delays and K the number of Doppler positions. In the time-frequency domain, L represents the number of subcarriers and K the number of multicarrier symbols, in this case FBMC symbols.

C. MATRIX NOTATION

In order to simplify the analytical calculations and allow a better explanation of some concepts, we will express the proposed system via a matrix notation. The multi-carrier transmission system, via a filter bank, can be characterized by a structure of blocks that consist of K multi-carrier symbols, where each symbol has L subcarriers. Let us first define the n-point DFT matrix $\mathbf{W}_n \in \mathbb{C}^{n\times n}$ as follows

$$\mathbf{W}_n = \left\{ e^{j2\pi kl/n} \right\}_{k,l=0}^{n-1} \quad (9)$$

Therefore, the data already precoded at the input of the filter bank modulator can be expressed in matrix format by

$$\mathbf{X} = \mathbf{C}_f \mathbf{A} \mathbf{W}_K^H, \quad (10)$$

where $\mathbf{A} \in \mathbb{C}^{L\times K}$ comes from the parallel-to-serial conversion of the data vectors $\mathbf{a} \in \mathbb{C}^{LK/\beta\times 1}$ followed by the mapping performed for the transmission strategy. Thus, this matrix contains QAM symbols in the first and last $L/2\beta$ lines and zeros elsewhere. The matrix $\mathbf{W}_K^H \in \mathbb{C}^{K\times K}$ represents the K-point IDFT matrix while $\mathbf{C}_f \in \mathbb{C}^{L\times L}$ is a matrix that consist of a L-point DFT $\mathbf{W}_L \in \mathbb{C}^{L\times L}$ and a filter compensation stage that will defined later. Note that from the set of IDFTs and DFTs that form the ISFFT ($\mathbf{W}_K^H$ and $\mathbf{W}_L$), we use the L-point DFT for the process of restoring the complex orthogonality. Making a direct connection between $a_{m,n}$ of (4) and $\mathbf{A}$, we can represent this matrix for a specific example with $L = 4$, $K = 4$ and $\beta = 2$ as follows:

$$\mathbf{A} = \begin{bmatrix} a_{0,0} & a_{2,0} & a_{0,1} & a_{2,1} \\ 0 & 0 & 0 & 0 \\ 0 & 0 & 0 & 0 \\ a_{1,0} & a_{3,0} & a_{1,1} & a_{3,1} \end{bmatrix} \quad (11)$$

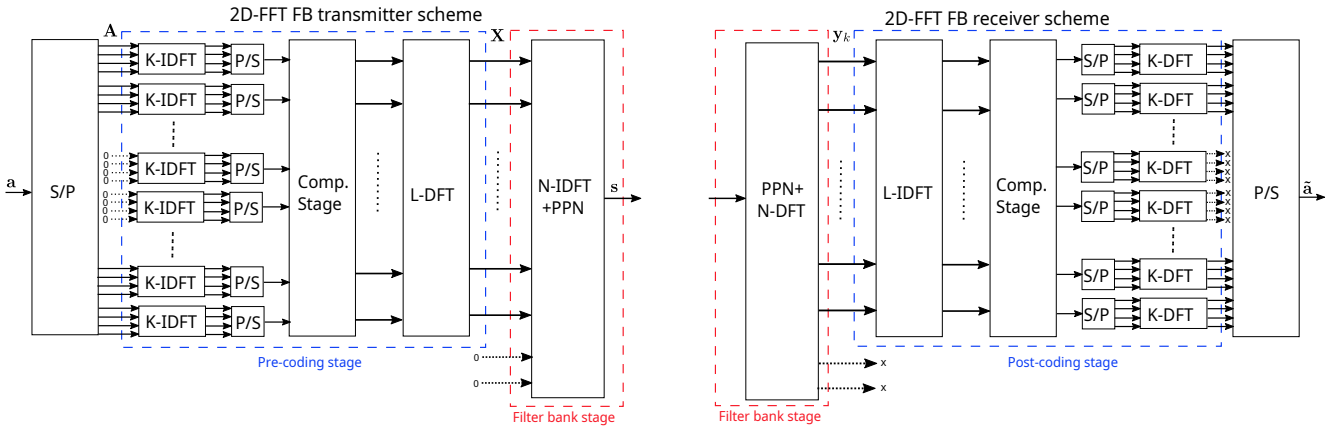

Figure 2: Block scheme of the 2D-FFT filter bank system.

This data allocation strategy is necessary to avoid filter interference and restore complex orthogonality, as we will see later in section II-D.

The filter bank system can be efficiently implemented through a polyphase network (PPN) combined with an IDFT and DFT [2]. Such an implementation significantly reduces the computational complexity compared to the direct implementation (one digital filter for each subchannel). The IDFT length N must be strictly higher than L, so that the DFT of the precoding stage does not cancel itself out with the IDFT of the filter bank. Thus, the IDFT from the filter bank is $\tilde{\mathbf{W}}_N^H \in \mathbb{C}^{N\times L}$ given by

$$\tilde{\mathbf{W}}_N = \begin{bmatrix}\mathbf{I}_L & \mathbf{0}_{L\times N-L}\end{bmatrix}\mathbf{W}_N. \tag{12}$$

Considering the transmission of K blocks where K is an integer of β, we can define a block IDFT matrix $\tilde{\mathbf{W}}^H \in \mathbb{C}^{NK\times LK}$, as

$$\tilde{\mathbf{W}}^H = \mathbf{I}_K \otimes \tilde{\mathbf{W}}_N^H, \tag{13}$$

where $\otimes$ refers to the Kronecker product which maps $\tilde{\mathbf{W}}_N$ to the correct time positions. Then, the transmitted data can be obtained by convolving the IDFT output by the prototype filter impulse response through a Toeplitz filter matrix. Let us consider the diagonal matrix $\mathbf{G}_p$ corresponding to the filter coefficients, that is, $\mathbf{G}_p = \text{diag}(\mathbf{g}_p) \in \mathbb{R}^{N/\beta\times N/\beta}$ for $p = 0, 1, 2, ..., \beta O - 1$, where $\mathbf{g}_p$ is given by $\mathbf{g}_p = [g[pN/\beta], g[pN/\beta+1], \ldots, g[pN/\beta+N/\beta-1]]$. First, let us define $\tilde{\mathbf{G}}_p \in \mathbb{R}^{N/\beta\times N}$ as follows:

$$\tilde{\mathbf{G}}_p = \big[\underbrace{\mathbf{0}_{N/\beta}\ \ \mathbf{0}_{N/\beta}\ \ \ldots}_{(p \bmod \beta)\text{ times}}\ \ \mathbf{G}_p\ \ \underbrace{\mathbf{0}_{N/\beta}\ \ \ldots\ \ \mathbf{0}_{N/\beta}}_{\beta-1-(p \bmod \beta)\text{ times}}\big] \tag{14}$$

where the number of arrays of zeros of size $N/\beta \times N/\beta$ around the coefficients array of the filter $\mathbf{G}_p$ depends on the value of p and β. Thus, the Toeplitz matrix of the filter $\mathbf{G} \in \mathbb{R}^{ON+(K-1)N/\beta\times NK}$ considering $K > \beta - 1$ multicarrier symbols can be expressed as:

$$\mathbf{G} = \begin{bmatrix}
\tilde{\mathbf{G}}_0 & \mathbf{0} & \mathbf{0} & \ldots & \mathbf{0} \\
\tilde{\mathbf{G}}_1 & \tilde{\mathbf{G}}_0 & \mathbf{0} & \ldots & \mathbf{0} \\
\tilde{\mathbf{G}}_2 & \tilde{\mathbf{G}}_1 & \tilde{\mathbf{G}}_0 & \ddots & \vdots \\
\vdots & \tilde{\mathbf{G}}_2 & \tilde{\mathbf{G}}_1 & \ddots & \mathbf{0} \\
\vdots & \vdots & \tilde{\mathbf{G}}_2 & \ddots & \tilde{\mathbf{G}}_0 \\
\tilde{\mathbf{G}}_{O\beta-1} & \vdots & \vdots & \ddots & \tilde{\mathbf{G}}_1 \\
\mathbf{0} & \tilde{\mathbf{G}}_{O\beta-1} & \ldots & \ddots & \tilde{\mathbf{G}}_2 \\
\vdots & \mathbf{0} & \tilde{\mathbf{G}}_{O\beta-1} & \ddots & \vdots \\
\vdots & \vdots & \vdots & \ddots & \vdots \\
\mathbf{0} & \mathbf{0} & \mathbf{0} & \ldots & \tilde{\mathbf{G}}_{O\beta-1}
\end{bmatrix}. \tag{15}$$

Once the transmission matrix to the precoded symbols has been defined, the output data vector $\mathbf{s}$ of length $M = ON + \frac{N}{\beta}(K-1)$ from the filter bank is given by

$$\mathbf{s} = \mathbf{G}\tilde{\mathbf{W}}^H\mathbf{x} = \bar{\mathbf{G}}\mathbf{x}, \tag{16}$$

where $\bar{\mathbf{G}} = \mathbf{G}\tilde{\mathbf{W}}^H \in \mathbb{C}^{M\times LK}$ and $\mathbf{x} = \text{vec}(\mathbf{X}) \in \mathbb{C}^{LK\times 1}$. The symbols are delayed between each N/β samples - the structure of $\mathbf{G}$ itself does this process transparently. The representation as a sum of matrices delayed among themselves can be seen in [9].

The transmitted signal vector $\mathbf{s}$ is affected by a time-varying multipath channel modeled by the convolution ma-

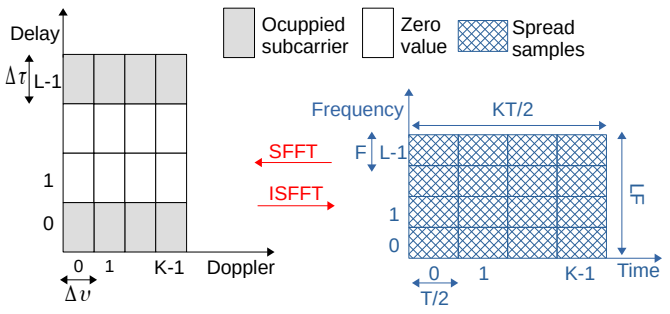

Figure 3: Analysis of time-frequency and delay-Doppler grids in the proposed scheme.

trix $\mathbf{H} \in \mathbb{C}^{M\times M}$ [15]. Thus, the received signal $\mathbf{r} \in \mathbb{C}^{M\times 1}$ is given by

$$\mathbf{r} = \mathbf{H}\mathbf{s} + \mathbf{n}, \tag{17}$$

where $\mathbf{n}$ has additive white Gaussian noise (AWGN) samples with zero mean and power σ_n^2. At the receiver, the reverse process of the transmitter is performed. Initially, the received signal is demodulated by the analysis filter $\mathbf{G}^T$ generating the vector $\mathbf{z} \in \mathbb{C}^{NK\times 1}$ expressed by

$$\mathbf{z} = \mathbf{G}^T\mathbf{r} \tag{18}$$

Then, through the DFT matrix $\tilde{\mathbf{W}}$, we obtain $\mathbf{y} \in \mathbb{C}^{LK\times 1}$, expressed as:

$$\mathbf{y} = \tilde{\mathbf{W}}\mathbf{z}, \tag{19}$$

For each position in the time-frequency grid, we have $y_{l,k} = [\mathbf{y}]_{l+Lk}$. To compensate for interferences coming from the channel and for the sake of simplicity, a one-tap frequency domain equalization process is performed by $\mathbf{e}_k \in \mathbb{C}^{L\times 1}$, originating $\tilde{\mathbf{x}}_k \in \mathbb{C}^{L\times 1}$ which is expressed as

$$\tilde{\mathbf{x}}_k = \text{diag}\{\mathbf{e}_k\}\mathbf{y}_k. \tag{20}$$

where $\mathbf{y}_k = [y_{0,k}\ y_{1,k}\ \dots\ y_{L-1,k}]^T \in \mathbb{C}^{L\times 1}$. Finally and considering all time instants, the detected symbols represented by $\tilde{\mathbf{A}} \in \mathbb{C}^{L\times K}$ are obtained through the SFFT combined with the compensation stage

$$\tilde{\mathbf{A}} = \mathbf{C}_f^H\tilde{\mathbf{X}}\mathbf{W}_K, \tag{21}$$

where $\tilde{\mathbf{X}} = [\tilde{\mathbf{x}}_0\ \tilde{\mathbf{x}}_1\ \dots\ \tilde{\mathbf{x}}_{K-1}] \in \mathbb{C}^{L\times K}$. In this way, we carry out a transmission based on precoding via two-dimensional FFT (2D-FFT) with the core of the system being a bank of filters. The idea now is to eliminate the imaginary interference coming from the filters using the encoding itself and consequently recover complex orthogonality.

D. RESTORATION OF COMPLEX ORTHOGONALITY

The FBMC/OQAM system provides an improvement in spectral localization with respect to regular OFDM through the subcarrier filtering process. However, this filtering generates interference and consequently the loss of complex orthogonality, complicating the use of MIMO techniques. By spreading the symbols we are able to cancel the filter interference, so all MIMO techniques can be applied directly to FBMC as in OFDM. The authors in [6] and [7] propose a precoding technique based on frequency spreading via DFT combined with a filter compensation stage in order to recover the complex orthogonality. In this scheme $L/2$ complex data symbols are spread over L subcarriers, leading to the same information rate as in conventional FBMC/OQAM. Thus, the data symbols no longer belong to a position on the specific frequency, but are spread over several subcarriers. Particularly in [7], where there is no need to use OQAM symbols, $L/2$ complex symbols are compensated by a scaling factor and are inserted in the first and in the last $L/4$ positions of a L-points DFT with the intermediate values equal to zero. This strategy is necessary to avoid filter interference in the frequency domain. At the receiver, we have the reverse process, where filter compensation and an L-points IDFT are performed.

The idea of the 2D-FFT FB system is that, starting from the precoding imposed by the ISFFT, interference from the filter can be eliminated only with the addition of a multiplicative compensation factor. Thus, it is necessary that the filter interference comes from only one coefficient. That is, only one pulse can interfere with the adjacent one. From (2) it is noted that the pulse duration, and consequently its number of coefficients, is controlled by the overlap factor O. The term O indicates the number of neighboring symbols the filter will overlap and cause interference. Thus, the filter size must be limited to avoid unneeded interference. To find the optimal size value, three base pulses will be analyzed. Considering $N = L$ and $\beta = 2$ without loss of generality, initially we consider that OL is the pulse width and $L/2$ is the pulse width selected for transmission. The idea is to avoid overlap between transmitted pulses in windows of length $L/2$, as shown in Figure 4. Since the selected pulse starts at a time $OL/2-L/4$, the complete pulse ends at OL; since we spread the symbols on a L-point DFT, we must have

$$\begin{aligned} OL - \left(\frac{OL}{2} - \frac{L}{4}\right) &\leq L \\ \frac{OL}{2} + \frac{L}{4} &\leq L \\ O &\leq \frac{3}{2} \end{aligned} \tag{22}$$

Therefore, the overlap factor must not be greater than $O = 1.5$ to avoid interference between symbols in the time domain. In this way, each symbol transmitted within a window of length $L/2$ will be multiplied by the sample value of a single pulse at each time instant. Figure 4 illustrates this approach. Note that for $O = 1.5$, the start of the third adjacent pulse is at the limit position, so it is interfering with only one pulse and, consequently, such interference is of only one coefficient. However, for $O = 2$, it can be seen that the third pulse starts to interfere with the first pulse, giving rise to an interference of more than one coefficient. Generalizing for any value of β, we arrive at the relationship between the overlap factor O and the rate factor β to avoid interference being described by

$$\begin{aligned} OL - \left(\frac{OL}{2} - \frac{L}{2\beta}\right) &\leq L \\ O + \frac{1}{\beta} &\leq 2 \end{aligned} \tag{23}$$

Furthermore, note that for β = 4 and 8 we can increase the overlap factor to 1.75 and 1.875, respectively. Depending on the filter being used, this small increase in the filter's overlap factor can be useful to decrease out-of-band emissions. However, in general this benefit of increasing β is not as significant in this aspect, as shown in Figure 5, which represents the frequency responses of the prototype filters

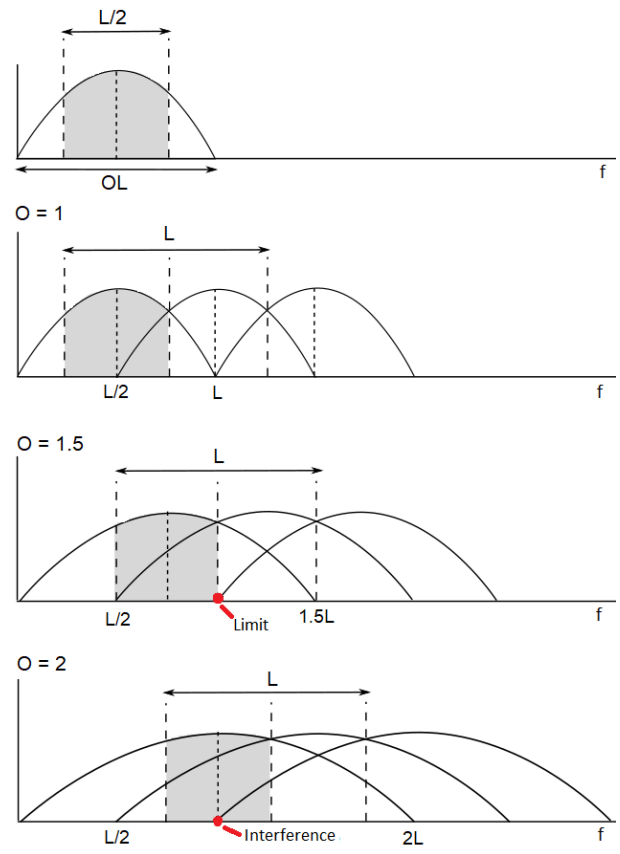

Figure 4: Limitation of the overlapping factor to $\beta = 2$.

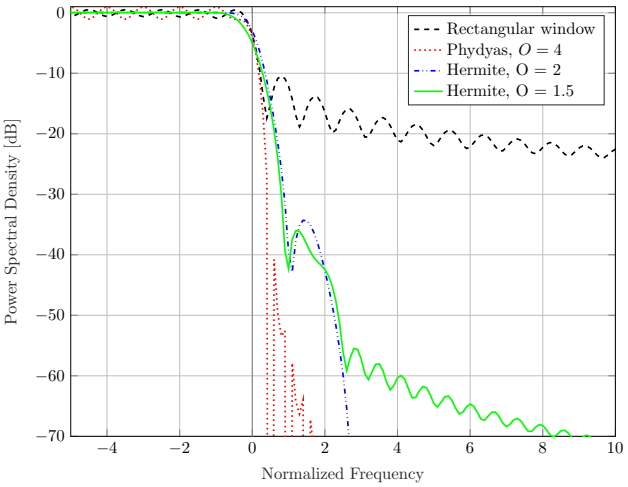

Figure 5: Power Spectral Density comparison between filters.

for different overlapping factors. To obtain a better filtering with these overlap factors it is necessary to design and optimize a filter specifically for them, and not just modify an already designed filter. We will see below that the main advantages of generalization of the filter bank structure and allowing different values of β are in terms of PAPR and error performance in high mobility scenarios.

Considering then that the overlapping factor is within the limits defined above, we can effectively define $\mathbf{C}_f$ to restore the complex orthogonality. As mentioned earlier, such a matrix consists of the filter compensation stage combined with the DFT L-point matrix present in the ISFFT, that is, [7]

$$\mathbf{C}_f = \mathbf{W}_L \text{diag}\{\tilde{\mathbf{b}}\}, \tag{24}$$

where $\tilde{\mathbf{b}} \in \mathbb{R}^{L\times 1}$ is the scale vector with L/β compensation coefficients in the positions according to the transmission strategy. In order to restore complex orthogonality, $\mathbf{C}_f$ must be chosen so that the following condition is achieved:

$$\mathbf{C}_f^H \tilde{\mathbf{W}}_N \widetilde{\mathbf{G}}^T \widetilde{\mathbf{G}} \tilde{\mathbf{W}}_N^H \mathbf{C}_f \approx \mathbf{F}, \tag{25}$$

where $\mathbf{F} \in \mathbb{R}^{L\times L}$ is a matrix with unit values in the first and last $L/2\beta$ positions of its main diagonal and zeros elsewhere. $\widetilde{\mathbf{G}}$ corresponds to the transmission of a single filter bank symbol, expressed by $\widetilde{\mathbf{G}} = [\mathbf{G}_0; \mathbf{G}_1; ...; \mathbf{G}_{\beta O-1}] \in \mathbb{R}^{ON\times N}$. Substituting (24) into (25), the $\tilde{l}$-th position of $\tilde{\mathbf{b}}$ can be expressed by

$$[\tilde{\mathbf{b}}]_{\tilde{l}} = \begin{cases} \sqrt{\frac{1}{[\tilde{\mathbf{c}}]_{\tilde{l}}}}, & \text{for } \tilde{l} = \left[0,\ldots,\frac{L}{2\beta}-1; L-\frac{L}{2\beta}-1,\ldots,L-1\right] \\ 0, & \text{otherwise} \end{cases} \tag{26}$$

with

$$\tilde{\mathbf{c}} = \text{diag}\{\mathbf{W}_L^H \tilde{\mathbf{W}}_N \widetilde{\mathbf{G}}^T \widetilde{\mathbf{G}} \tilde{\mathbf{W}}_N^H \mathbf{W}_L\}. \tag{27}$$

Figure 6 shows the reason for the transmission strategy used and how $[\tilde{\mathbf{c}}]_{\tilde{l}}$ depends on position $\tilde{l}$. Note that half of the symbols in each subcarrier is amplified ($[\tilde{\mathbf{c}}]_{\tilde{l}} > 1$), while the remainder is attenuated. Thus, the proposed solution is to transmit where $[\tilde{\mathbf{c}}]_{\tilde{l}} > 1$. Consequently, the data symbols are inserted in the corresponding first and last $L/2\beta$ positions of the DFT. The transmission rate L is maintained by rate factor β. The proposed transmission idea is to transmit in the $L/2$ larger elements of $\tilde{\mathbf{c}}$ in the case $\beta = 2$. Therefore, this strategy combined with precoding allows us to use QAM modulation and relax filter restrictions in order to obtain more efficient filtering, better resource allocation and even an extension of the overlapping factor limit. On the receiver

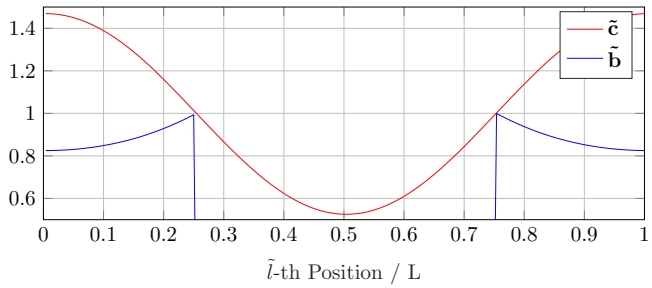

Figure 6: Illustration of vectors $\tilde{\mathbf{b}}$ and $\tilde{\mathbf{c}}$ for $\beta = 2$.

side we only consider the positions in which the transmitted symbol is retrieved. With this, equalization becomes simpler since the symbols are now free from filter interference. Due to its similarity to OTFS, the same detection techniques proposed and implemented in the OTFS technique can be

applied to the 2D-FFT FB one. However, the use of frequency domain equalizers, such as the one-tap used in OFDM systems, have much better performance in 2D-FFT FB [10].

E. LINK WITH OTFS TECHNIQUE

As previously discussed and described, the technique proposed in this work has the same basic encoding process that the one performed in the OTFS technique through an ISFFT. However, in our scheme the transmission is performed by a filter bank at a rate β in order to obtain the same symbol density as the OTFS technique, since only L/β of the L delay positions in the grid are active. For this to be possible, our scheme is using β times more Doppler positions than the OTFS technique. The question that remains is whether there is any difference between the Doppler resolution obtained in our proposed structure ($\Delta\nu = \frac{1}{KT/\beta}$) compared with the OTFS Doppler resolution. If K is the number of Doppler positions for the 2D-FFT FB and the transmission is performed at a rate T/β, to obtain the same density of transmitted data, we have K/β Doppler positions in the OTFS technique, each of which is transmitted at a rate T. Consequently, the Doppler resolution for the OTFS is given by $\frac{1}{KT/\beta}$, that is, the same as the one of the generalized 2D-FFT FB. The main difference is that the OTFS transmission is performed at rate T while the number of transmitted Doppler positions is reduced to K/β. In this way, we have the same symbol density transmitted between the techniques, in addition to the same Doppler resolution. Therefore, a fair comparison can be made between them. Figure 7 presents a comparison between the delay-Doppler grids for both techniques. Note that we have a compromise: we do not use all the positions in the delay domain so that it is possible to restore the complex orthogonality. However, in the Doppler domain we have the same resolution obtained in the OTFS with the addition of a dynamic range β times greater. We slightly reduce the robustness to delay spread, while considerably increasing the robustness to Doppler spreading. Such a configuration becomes plausible nowadays, where scenarios with high Doppler spreading or applications in millimeter waves are major study focuses.

Such an analysis can also be seen by the time-frequency grids. In a conventional OTFS transmission, a delay-Doppler grid of size $L \times K/\beta$ is transformed into a time-frequency grid $K/\beta \times L$ through the ISFFT and transmitted by an OFDM modulator. In the generalized 2D-FFT FB technique, a $L \times K$ delay-Doppler domain grid, with only $L/\beta \times K$ active positions, is transformed into a $K \times L$ frequency-time-domain grid, as illustrated in Figure 3. Finally, this grid is divided into β grids of size $K/\beta \times L$ (same as OTFS). Each grid is processed by the PPN and finally summed with their respective delays, obtaining the transmission at a rate T/β. Figure 8 illustrates the procedure performed in the transmission via filter bank for $\beta = 4$. Each colored block corresponds to $L/4$ information data spread over L subcarriers. In a OTFS time slot, L complex symbols are transmitted. In our proposed system with the rate factor, $L/4$ complex

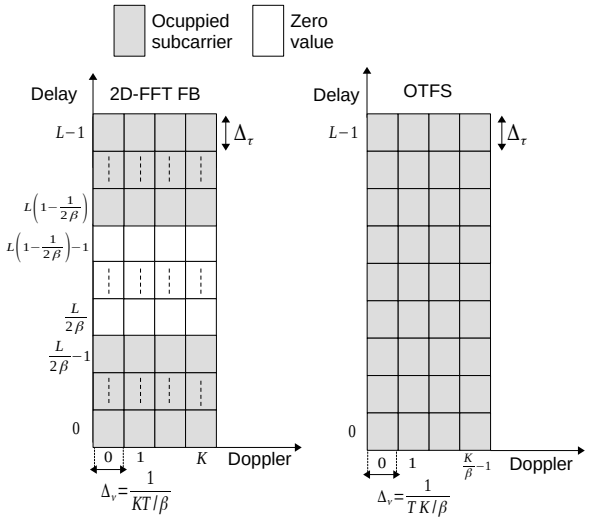

Figure 7: Analysis of delay-Doppler grids in the proposed scheme and OTFS.

symbols are transmitted in 4 time slots. It is worth mentioning that this transmission structure is realized transparently by $\mathbf{G}$ presented in (15). Clearly, by the Figure of the proposed system and equations (1) and (8), we can see the difference of the proposed system when compared to the conventional OTFS. Now, the transmission is performed through a filter bank at a rate β and the complex orthogonality recovery part based on spreading via DFT is used to implement the symplectic transform.

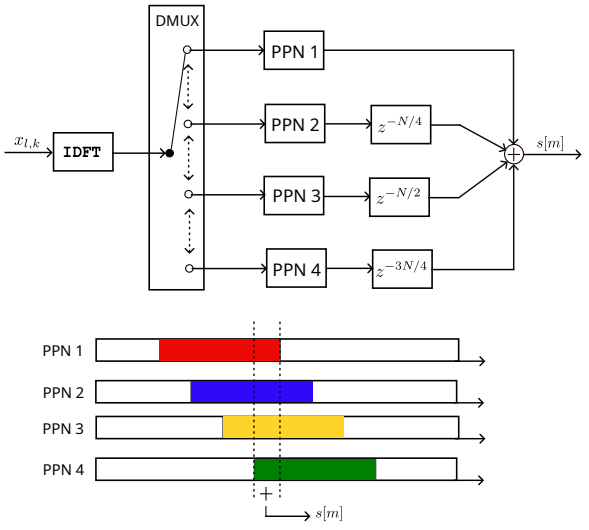

Figure 8: Transmission structure via filter bank at rate $\beta = 4$

III. EQUALIZATION IN TIME-FREQUENCY DOMAIN

To obtain maximum diversity in OTFS, receivers in the delay-Doppler domain are used. However, these receivers are more complex when compared to the simple one-tap equalizer in the time-frequency domain of the OFDM system. The ML detector is ideal in the sense that it minimizes the probability

of error [16]. Despite the great performance it offers, this method is not attractive for high data rate situations that employ large order modulations. Therefore, in practice, linear equalization is considered to obtain an estimate of the transmitted symbol sequence with low complexity [17]. As seen in [10] such equalizers for OTFS do not have good performance. This is not the case for 2D-FFT FB system, due to the filtering process. The idea here is to explore TF equalizers combined with the proposed rate factor in 2D-FFT FB systems.

A. ONE-TAP EQUALIZER

To find the TF one tap equalizer coefficients, we first define the channel coefficients for the respective points in the TF domain from $\mathbf{D} \in \mathbb{C}^{LK \times LK}$, expressed as

$$\mathbf{D} = \bar{\mathbf{G}}^H \mathbf{H} \bar{\mathbf{G}}. \tag{28}$$

Thus, we can then represent the one-tap channel by $\mathbf{h} = \text{diag}\{\mathbf{D}\} \in \mathbb{C}^{LK \times 1}$ [9]. Considering each sample in time and frequency, we have $h_{l,k}$ expressed by

$$h_{l,k} = [\mathbf{h}]_{l+Lk}. \tag{29}$$

From this definition, a simple one-tap zero forcing (ZF) equalizer is provided by $(1/h_{l,k})$. To obtain a balanced solution between noise and channel interference, we employ the equalizer based on the MMSE criterion, which can be expressed as follows:

$$e_{l,k} = \frac{h_{l,k}^*}{|h_{l,k}|^2 + \sigma_n^2}. \tag{30}$$

If delay propagation and Doppler propagation are low enough, a one-tap equalizer is sufficient to compensate for channel interference.

B. ITERATIVE EQUALIZER

Alternatively, we can use more robust receivers that can improve performance especially in high mobility scenarios. In [18], such an iterative scheme was adopted which can strongly compensate for channel interference at the expense of somewhat greater receiver complexity. Another type of receiver with feedback to eliminate residual interference can be used. For our case where the equalization is done in the frequency domain, the use of this type of receiver in the iterative format proves to be feasible and simple. This fact motivates the use of the iterative block decision feedback equalization (IB-DFE), where already equalized symbols are used to improve the reliability of those detected at each iteration [18].

The IB-DFE structure is iterative, with both the feedforward (FF) and feedback (FB) filters in the frequency domain [19]. In this scheme, already equalized symbols are used to improve the reliability of the detected ones at each iteration. It was seen that a small number of iterations is needed to reach a considerable performance advantage with respect to standard one-tap frequency domain equalizers. Figure 9 presents the iterative equalizer adapted for the 2D-FFT system. In a first instant, the received symbols pass through the MMSE equalizer and the post-coding process (SFFT + compensation stage) of the system is carried out. After post-coding, the symbols are detected and returned to the time-frequency domain by an ISFFT in an iterative process. In this process, the symbols are filtered by a feedback filter in order to eliminate residual interference. Thus, the symbol estimate $\tilde{\mathbf{x}}^i$ for the i-th iteration is formed by

$$\tilde{\mathbf{x}}^i = \dot{\mathbf{y}}^i + \ddot{\mathbf{y}}^i, \tag{31}$$

where $\dot{\mathbf{y}}^i \in \mathbb{C}^{LK \times 1}$ is the output of the feedforward filter in the i-th iteration and is given by

$$\dot{\mathbf{y}}^i = \mathbf{P}^{i,H} \mathbf{y}, \tag{32}$$

with $\mathbf{P}^{i,H} \in \mathbb{C}^{LK \times LK}$ corresponds to the feedforward filter that aims to maximize the SINR of the detected symbols at each iteration. The vector $\ddot{\mathbf{y}}^i \in \mathbb{C}^{LK \times 1}$ is the output of the feedback filter, and it can be expressed as

$$\ddot{\mathbf{y}}^i = \mathbf{Q}^{i,H} \hat{\mathbf{x}}^{i-1}, \tag{33}$$

where $\mathbf{Q}^{i,H} \in \mathbb{C}^{LK \times LK}$ is the matrix corresponding to the feedback filter and $\hat{\mathbf{x}}^{i-1} \in \mathbb{C}^{LK \times 1}$ is the frequency domain estimated vector after symbol decision. The role of this feedback filter is the removal of the residual inter symbol interference (ISI). Let us define a matrix for the one-tap channel coefficients $\mathbf{h}$ as $\overline{\mathbf{H}} = \text{diag}\{\mathbf{h}\} \in \mathbb{C}^{LK \times LK}$. Now, to obtain the coefficients for both the feedforward and the feedback filter at the i-th iteration, the goal is to minimize the mean square error (MSE), conditioned on $\overline{\mathbf{H}}$, in the following way:

$$MSE^i = \quad E_{\overline{\mathbf{H}}}[||\mathbf{P}^i \mathbf{y} + \mathbf{Q}^i \hat{\mathbf{x}}^{i-1} - \mathbf{a}||^2], \tag{34}$$

where $\mathbf{a} \in \mathbb{C}^{LK \times 1} = vec(\mathbf{A})$. In order to simplify this process we assume, as in [7], that we have ideal feedback after the first iteration. Thus, by imposing the constraint that the feedback filter removes the ISI but not the desired symbol, by minimizing the MSE expressed by (34) we obtain the coefficients of the filters $\mathbf{P}^i$ and $\mathbf{Q}^i$, which are given by:

$$\mathbf{P}^i = \mathbf{R}_{\mathbf{yy}}^{-1} (\mathbf{I}_{LK} - \mathbf{Q}^i) \mathbf{R}_{\mathbf{ya}}, \tag{35}$$

and

$$\mathbf{Q}^i = -[\mathbf{R}_{\mathbf{ay}} \mathbf{P}^i - \rho \mathbf{I}_N], \tag{36}$$

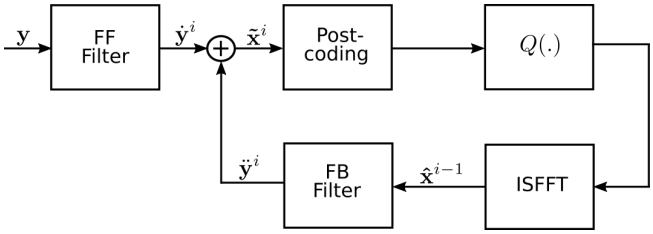

Figure 9: Block scheme of the iterative equalizer.

where ρ is given by

$$\rho = \frac{\text{Tr}[\mathbf{R_{ay}}\mathbf{P}^i]}{LK}. \tag{37}$$

The matrices $\mathbf{R_{yy}}, \mathbf{R_{ya}}$ and $\mathbf{R_{ay}}$ all of size $LK \times LK$ are expressed by

$$\mathbf{R_{yy}} = \overline{\mathbf{H}}\overline{\mathbf{H}}^H + \sigma_n^2 \mathbf{I}_{LK}, \tag{38}$$

$$\mathbf{R_{ya}} = \overline{\mathbf{H}}, \tag{39}$$

and

$$\mathbf{R_{ay}} = \overline{\mathbf{H}}^H \tag{40}$$

which are respectively the correlation matrices between the received symbols themselves, between the received and transmitted symbols and vice versa. Since the accurate estimation of the symbol correlation matrices $(\hat{\mathbf{x}}^{i-1})$ is a complex process, we can simplify this estimation by considering that the feedforward filter will perform well in the first iteration. That is, we are assuming that the feedback decisions will be correct. With this, immediately after the first iteration the feedforward filter is switched to the matched filter. We remind that at the first iteration $(i = 1)$ $\mathbf{Q}^1 = 0$, due to the lack of previous decisions; therefore, $\mathbf{P}^1$ is also reduced to

$$\mathbf{P}^1 = \mathbf{R}_{\mathbf{yy}}^{-1}\mathbf{R_{ya}}, \tag{41}$$

i.e., the frequency domain MMSE equalizer [9]. As can be seen in [10], the one-tap equalizer in the frequency domain for conventional OTFS brings much lower performance when compared to the one obtained with our proposed 2D-FFT technique. This fact makes the proposed IB-DFE inappropriate to use with OTFS, due to the unreliable first estimates of the direct filter provided for the feedback filter in the iterative process.

Table 1 presents the computational complexity of the proposed structure, together with those of the MMSE equalizers in the TF and DD domain and the Approximate message passing simplified by First Order (AMP-FO) proposed by [20]. The addition of this last receiver is interesting for comparison, as it is a robust algorithm and is an approximation of conventional MPA, widely proposed and studied in OTFS systems. Clearly, the one-tap equalizer in the TF domain is the simplest. On the other hand, the MMSE solution in the DD domain, using the traditional matrix inversion, requires the greatest complexity [10]. For the IB-DFE equalizer, due to the iterative process the term $\bar{i}$ is the maximum number of iterations used, while $(LK\log(L/\beta) + (L/\beta)K\log K)$ represents the complexity of SFFT. In addition to the size of the delay-Doppler grid, the complexity of the AMP-FO receiver is calculated as a function of the constellation size Z-QAM, the number of the channel taps, P and also the number of iterations used in the algorithm [21]. Although the order of the AMP-FO and IB-DFE receivers are similar (linear), the computational implementation of AMP-FO has a much greater complexity due to the number of operations performed by the algorithm. Furthermore, a much larger number of iterations is required in AMP-FO than in IB-DFE for similar error performance.

Receiver	Complexity
MMSE - TF domain	$O(LK)$
MMSE - DD domain	$O(L^3K^3)$
IB-DFE	$O(i LK\log(L/\beta) + i(L/\beta)K\log K)$
AMP-FO	$O(iLKP + iLKZ)$

Table 1: Computational complexity of the receivers.

In terms of system complexity, Table 2 presents the computational complexity of the conventional 2D-FFT transmitter, i.e. $\beta = 2$ and for the generalized case. Directly highlighting the generalized version, we have $K' = \frac{\beta K}{2}$ multicarrier symbols each with L/β subcarriers. Thus, for each symbol, L/β multiplications referring to the compensation stage are required. The term K' for the generalized version is needed to obtain the same amount of transmitted data symbols for a fair comparison with the conventional model. Furthermore, the term $N\log N + ON$ corresponds to the modulator via a filter bank implemented from an N-point IFFT combined with the ON multiplications of the prototype filter. The term $L\log(L/\beta) + (L/\beta)\log(K')$ ISFFT composed of an L-point FFT together with a K'-point FFT resulting in the term. If we consider the ratio between the complexity of the generalized version and the conventional version, we have an increase in transmitter complexity of approximately 1.8 and 3.6 times for $\beta = 4$ and $\beta = 8$ respectively. It will be seen later on that there is a good trade-off between complexity and error performance.

Scheme	Complexity
2D-FFT FB	$K(\frac{L}{2} + L\log(L/2) + (L/2)\log(K) + N\log N + ON)$
2D-FFT FB G	$K'(\frac{L}{\beta} + L\log(L/\beta) + (L/\beta)\log(K') + N\log N + ON)$

Table 2: Computational complexity of transmission scheme.

IV. ERROR PERFORMANCE ANALYSIS

In order to analyze the channel-induced interference and the robustness of the proposed system, in this section we will formally derive expressions for SINR, SIR and bit error probability (BEP). The analysis is made only for the one-tap equalizer, due to the relatively high computational complexity for OTFS and IB-DFE receivers. Simulation results will be presented for these latter receivers. Performing a parallel-serial conversion to $\tilde{\mathbf{A}}$ in (21), the input-output ratio of the entire transmission system defined by $\tilde{\mathbf{a}} \in \mathbb{C}^{LK\times 1}$ can be modeled by

$$\tilde{\mathbf{a}} = \underbrace{\mathbf{C}^H\text{diag}\{\mathbf{e}\}\bar{\mathbf{G}}^H\mathbf{H}\bar{\mathbf{G}}\mathbf{C}}_{\mathbf{\Delta}}\mathbf{a} + \underbrace{\mathbf{C}^H\text{diag}\{\mathbf{e}\}\bar{\mathbf{G}}^H}_{\mathbf{\Upsilon}}\mathbf{n}. \tag{42}$$

where $\mathbf{C} \in \mathbb{C}^{LK\times LK}$ corresponds to the system coding process for all transmitted blocks and is given by performing

$$\mathbf{C} = (\mathbf{I}_K \otimes \mathbf{C}_f)(\mathbf{W}_K^H \otimes \mathbf{I}_L). \tag{43}$$

The off-diagonal values of $\mathbf{\Delta} \in \mathbb{C}^{LK\times LK}$ and $\mathbf{\Upsilon} \in \mathbb{C}^{LK\times M}$ represent the interference induced due to channel and noise,

respectively. Finally, $\mathbf{e} \in \mathbb{C}^{LK\times 1}$ is the column vectorization of all elements of $\mathbf{e}_k$. Considering the independent and identically distributed transmitted symbols of zero mean and unity power and without statistical relation to noise, the SINR conditioned on a given channel realization $\mathbf{H}$ can be calculated according to:

$$\text{SINR}_{l,k}(\mathbf{H}) = \frac{1}{\sum_{i=0}^{LK-1}\left|[\mathbf{\Delta}-\mathbf{I}]_{\rho,i}\right|^2 + \sigma_n^2\sum_{i=0}^{M-1}\left|[\Upsilon]_{\underline{lk},i}\right|^2}, \quad (44)$$

with $\rho = Lk + l$ describing the ρ-th position of the line corresponding to the subcarrier l and the time instant k.

Through the SINR expression it is possible to calculate the instantaneous bit error probability (BEP) (i.e. the BEP for a given channel realization). Thus, assuming Gaussian approximation is used for the interference, the BEP to each channel realization can be obtained according to

$$\text{BEP} = E_{\mathbf{H}}\left\{\frac{1}{K}\sum_{k=0}^{K-1}\frac{1}{L/\beta}\sum_{l}\text{BEP}_{\text{AWGN}}\{\text{SINR}_{l,k}(\mathbf{H})\}\right\} \quad (45)$$

where BEP_{AWGN} is the BEP for the case of an AWGN channel, which is more precisely specified in [15], and the expectation $E_{\mathbf{H}}$ is obtained through the Monte Carlo simulation. The error probability is obtained by averaging all the conditional error probabilities corresponding to the channel realizations. In general, the larger the value of L the more valid the Gaussian approximation for the interference will be. Moreover, we will use a full DFT with the addition of zeros in the data vector, $\mathbf{\Delta}$ and Υ will have dimensions $LK \times LK$, but with $LK/\beta \times LK/\beta$ non-null values.

A time-varying channel, with strong Doppler spread, can lead to significant interference effects. To describe only the influence of a doubly selective channel, we will ignore the noise and remove the equalizer at $\mathbf{\Delta}$, resulting in $\bar{\mathbf{\Delta}} = \mathbf{C}^H\bar{\mathbf{G}}^H\mathbf{H}\bar{\mathbf{G}}\mathbf{C}$. Evaluating the entire received block, we can calculate the SIR dependent on the channel realization as follows:

$$\text{SIR} = \frac{\left|\text{diag}\{\bar{\mathbf{\Delta}}\}\right|^2}{\sum_{i=1}^{LK}\left|[\bar{\mathbf{\Delta}}]_{\underline{lk},i}\right|^2 - \left|\text{diag}\{\bar{\mathbf{\Delta}}\}\right|^2}. \quad (46)$$

Doubly selective channels are characterized by off-diagonal non-null values in $\bar{\mathbf{\Delta}}$. On the other hand, diagonal elements describe the desired signal components. Figures 10 and 11 show how the SIR changes for ITU-T Pedestrian A and Vehicular A channels [22] considering different velocity values and for a subcarrier spacing of $F = 15$KHz, respectively.

For the Pedestrian A channel model it can be seen that even at high speeds, such as 300 km/h, the SIR remains at a sufficiently high level, mainly in the cases where $\beta = 4$ and 8. It is possible to observe that we have a SIR gain of 7 dB by changing β from 2 to 4 in this scenario. The behavior is similar for the Vehicular A channel, when compared to the previous scenario, but with a worse SIR performance due to the channel model being more selective, inducing more interference. Finally, it can be seen that for both cases, we have an increase in the SIR level when increasing β, with the SIR values decreasing more slowly when increasing speed.

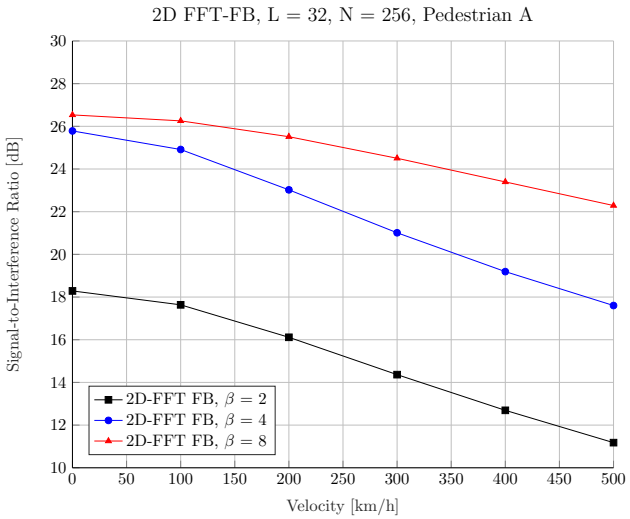

Figure 10: SIR analysis against velocity for Pedestrian A channel model.

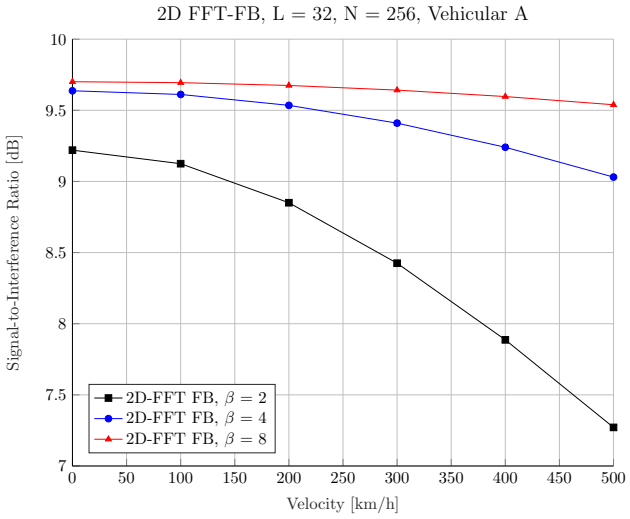

Figure 11: SIR analysis against velocity for Vehicular A channel model.

The introduction of the rate factor allows using the 2D-FFT FB system in high mobility scenarios, obtaining better performance. The waveform itself is compatible with the OTFS technique in addition to obtaining lower OOB emissions [10]. As we will see, unlike the OTFS technique, equalizers in the TF domain have a good BER performance in addition to allow a receiver with lower complexity. In terms of filter bank based systems, our proposal eliminates the interference of the filtering process allowing the use of MIMO techniques. In particular, Alamouti space-time block code and ML MIMO detection become feasible. This is also true for the schemes presented in [5] and [6]; however, the highest performance in doubly selective channels is achieved in the 2D-FFT FB scheme.

V. NUMERICAL RESULTS

In order to validate the proposed system, simulation results will be provided in this section. The Monte Carlo simulation method was chosen due to its simplicity. The transmitted signal is affected by a Rayleigh fading channel using the ITU-T Vehicular A model, while perfect channel estimation is assumed at the receiver. The total number of subcarriers is 1024, which leads to the condition

$$\frac{LK}{\beta} = 1024. \tag{47}$$

Remembering that K corresponds to the number of subbands (multicarrier symbols in time) and L to the number of subcarriers per subband. In order to keep the same number of transmitted symbols, we set L at 128 and vary the value of K according to the condition of the equation (47). Note that the value of K must be adjusted to maintain the same density of transmitted symbols at rate L/β [9]. We highlight that in all our comparisons the same block duration was adopted for all schemes. All the presented techniques are compared through the BER performance. The theoretical BER curves for the MMSE one-tap equalizer in TF domain (MMSE-TF) were obtained using the equation (45) for both the DFT precoded filter bank [7] and 2D-FFT FB schemes. These BER curves were compared with the ones obtained through Monte Carlo simulation using differents rate factor values. These rate factors were also used to simulate the IB-DFE equalizer with four iterations. Only 4 iterations are used for this equalizer, since there is no significant performance gain for more iterations. Simulation results also were obtained and compared for OTFS systems using different detection techniques: MMSE delay-Doppler (MMSE-DD) domain, MMSE-TF, IB-DFE and AMP-FO. The last one operates iteratively with 12 iterations and a damping factor of 0.6 as used in [21]. AMP-FO and MMSE-DD were also applied to the 2D-FFT FB scheme in order to demonstrate its compatibility with OTFS.

The filter used for the filter bank systems is the Hermite one, detailed in [23] and is based on a Gaussian function; therefore, it has a good location in the time-frequency plane. We consider a truncated version from $O = 2$ to 1.5 in order to avoid the interferences caused by it in the system. The remaining simulation parameters are shown in Table 3. In order to compare the effectiveness of the rate factor in precoded filter bank systems, Figure 12 shows the BER for 4-QAM modulation and a speed of 400 km/h for DFT

Parameters	
Total number of Subcarriers (L)	128
Rate factor (β)	2,4 and 8
Multi-carrier Symbols (K)	8β
Filter Bank FFT Size (N)	256
Modulation	4-QAM and 16-QAM
Channel Model	ITU-T Vehicular A
Velocity (V)	0, 300 and 400 Km/h
Subcarrier spacing (F)	15 kHz

Table 3: Simulation parameters.

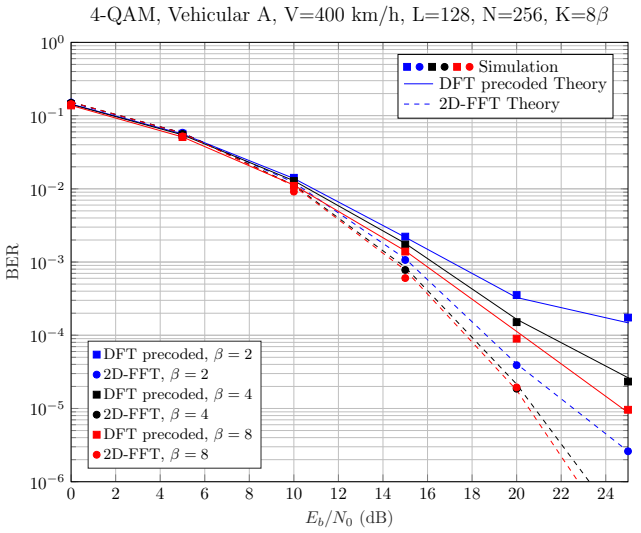

Figure 12: Error performance comparison for 4-QAM and a velocity of 400 km/h using the MMSE-TF equalizer.

Precoded and 2D-FFT filter bank both varying the rate factor and using the MMSE-TF equalizer. The continuous and dotted curves present the semi-analytical analysis for DFT Precoded and 2D-FFT cases respectively. Through frequency spreading, the pulses become shorter in time and therefore more robust to time variations. Furthermore, the introduction of the rate factor β results in symbols with shorter duration that consequently will be more tolerant to interference caused by Doppler dispersion. It is possible to see a significant performance gain when the rate factor varies from $\beta = 2$ to 4 and 8. Such performance gain is more significant for the 2D-FFT filter bank system due its inherent Doppler robustness. Note that for $\beta = 8$ the DFT precoded filter bank system has lower performance than 2D-FFT with $\beta = 2$, showing this characteristic. The SIR analysis of Section IV gives us a good indication of the behavior of the system in the scenarios shown with respect to the variation of the rate factor β. From $\beta = 2$ to $\beta = 4$ there is a substantial performance gain, whereas from $\beta = 4$ to $\beta = 8$ the gain is reduced, as seen in Figures 10 and 11. As presented in Figure 12 there is no substantial performance gain when β goes from 4 to 8, we chose $\beta = 4$ for the next analysis, due to the better compromise between performance and complexity. Finally, it is noted that the theoretical curves practically correspond to the simulation ones, validating the system performance analysis presented in this work. The small variations between theoretical and simulated curves at high SNR values come from the fact that the channel interference is not purely Gaussian at this stage.

Applying the other receivers and now considering the OTFS technique, Figure 13 presents the BER curves for the same scenario presented in Figure 12. Initially, it is interesting to note the lower performance of OTFS using the MMSE-TF equalizer. For this reason, the application of the IB-DFE equalizer will present an error floor at high SNR, a fact that

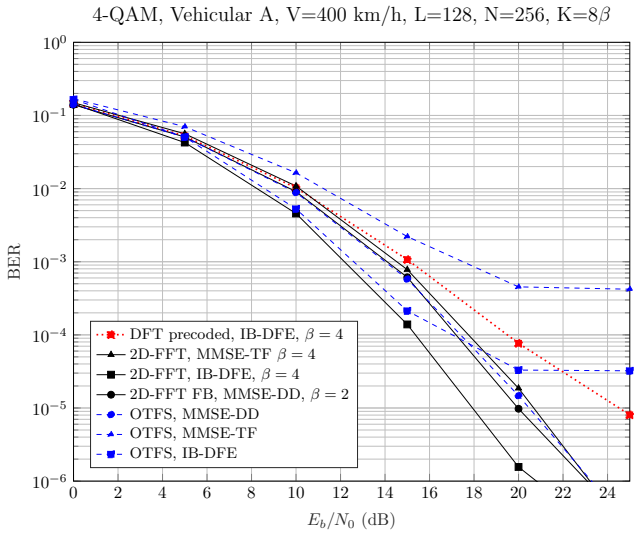

Figure 13: Error performance comparison for 4-QAM and a velocity of 400 km/h.

does not occur for the 2D-FFT FB - where we have the best performance among the obtained curves. Compared to OTFS with the computationally complex MMSE-DD equalizer, our proposed system using the low complexity MMSE-TF equalizer and $\beta = 4$ has similar error performance, thus validating the proposed scheme. Furthermore, the proposed IB-DFE equalizer has a performance gain of approximately 3 dB for a BER of 10^{-5} when compared to the OTFS with MMSE-DD. Finally, it is noted that the 2D-FFT FB using the same MMSE-DD equalizer and $\beta = 2$ also performs similarly to the OTFS with MMSE-DD, showing compatibility between the techniques.

Figure 14 presents the same comparison, but now for 16-QAM and a speed reduced to 300 km/h. In addition, the

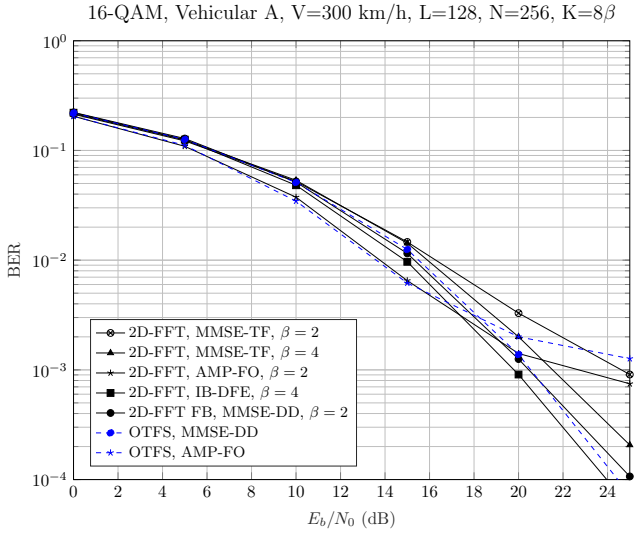

Figure 14: Error performance comparison for 16-QAM and a velocity of 300 km/h.

AMP-FO receiver is applied for the OTFS and 2D-FFT FB. As can be seen, OTFS with the AMP-FO technique slightly outperforms our schemes with one-tap equalizers (MMSE-TF and IB-DFE) for Eb/N0 lower than 16 dB. On the other hand, the IB-DFE equalizer with 4 iterations and $\beta = 4$ outperforms all others techniques for Eb/N0 greater than 17 dB. Moreover, let us note that the 2D-FFT scheme was implemented using the AMP-FO technique with $\beta = 2$ and obtained better BER performance than OTFS AMP-FO, demonstrating again the compatibility of the proposed scheme with OTFS. The performance will certainly be even better for higher values of β and this receiver. Finally, for this order of modulation the MMSE-TF equalizer for the 2D-FFT FB with $\beta = 4$ obtains a lower performance when compared to the MMSE-DD. However, the complexity of the MMSE-TF equalizer is drastically lower, thus achieving a good compromise on performance.

Let us now analyze the power variability of the transmitted vector $\mathbf{s}$ (equation 16). In particular, let us look at the PAPR which can be given by

$$PAPR = \frac{\max(|\mathbf{s}|^2)}{E[|\mathbf{s}|^2]}. \tag{48}$$

The PAPR measures the relationship between the peak power and the average power of a signal. A high PAPR indicates that the signal has high power spikes in relation to the average power, which can be undesirable in some communication systems. Figure 15 illustrates a comparison of the Complementary Cumulative Distribution Function (CCDF) of the PAPR considering the proposed structure, OFDM, OTFS and FBMC systems, for a 4-QAM signal constellation and $L = 256$ subcarriers. Note that 2D-FFT for $\beta = 2$ has similar performance to OTFS. This result is due to the use of DFT in the precoding scheme of both systems, which cancels out the IDFT of the OFDM transmitter used in the OTFS technique and also produces a similar effect in the 2D-

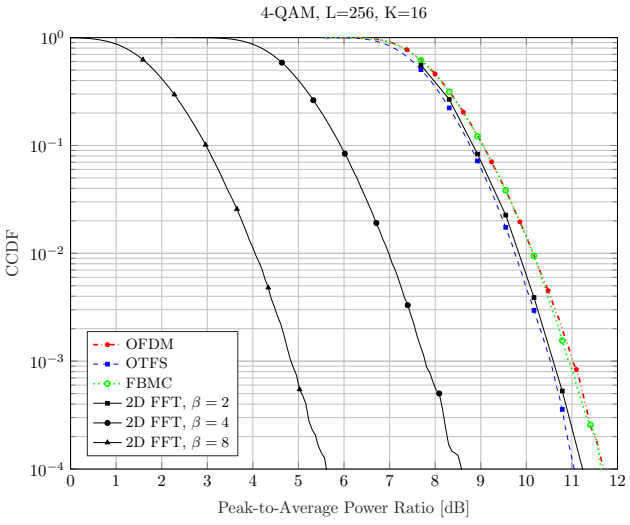

Figure 15: PAPR analysis between waveforms.

FFT FBMC transmitter. For this reason the PAPR in these systems does not depend on the number of subcarriers, but on the size K of the block to be transmitted. Nevertheless, their PAPR is smaller when compared to OFDM and FBMC. Furthermore, for the 2D-FFT FB, Figure 15 shows that by increasing the rate factor β to 4 and 8 there is a PAPR reduction of approximately 3 dB between each variation. This is expected, because with each increase in β there is a reduction of half of the symbols to be transmitted per block with a corresponding reduction of the transmission's time interval. Thus, it is possible to use the rate factor to tune the PAPR of the 2D-FFT FB system to better cope with transmitters sensitive to high PAPR.

VI. CONCLUSION

Wireless data transmission on time-varying channels and with high Doppler dispersion is challenging. The robustness of the OTFS technique to highly dynamic and complex scenarios makes it attractive to use in future wireless communications that support a wide range of emerging applications. This work aims to obtain a system with the same robustness of OTFS, but with the advantage of achieving equalization with good performance and low complexity in the TF domain, in addition to lower OOB and PAPR. Thus, we have presented a new precoded filter bank structure based on spreading in time and frequency which presented significant advantages in double selective channels. Furthermore, with a flexible data allocation strategy a generalization of the waveform structure was studied to make changes in the transmission of symbols through the filter bank. A clear and concise matrix analysis that allows a system analysis in terms of SIR and SINR was presented to validate the advantages of the proposed system. Finally, a performance comparison was made between the proposed scheme with other multi-carrier systems.

This work opens several aspects to be addressed in the future, such as an expansion to the case of using MIMO techniques and more aggressive channels in terms of time spreading. Moreover, channel estimation for the proposed structure is also an open challenge. The application of other receivers proposed for the OTFS technique, such as those based on MPA, is an interesting topic to work on. Further comparisons can be made in terms of performance, complexity and compatibility with the system proposed in this work. The complexity analysis and a more concise simplification in relation to the precoding process - more precisely, the DFT with the multi-carrier core represented by the IDFT - is another interesting topic to be addressed. Finally, it would be interesting to compare the proposed structure with other waveforms and the use of filters designed for smaller overlap factors in order to benefit from the extended rate limit.

References

[1] F. Boccardi, R. W. Heath, A. Lozano, T. L. Marzetta, and P. Popovski, "Five disruptive technology directions for 5G," IEEE communications magazine, vol. 52, no. 2, pp. 74–80, 2014.

[2] P. Siohan, C. Siclet, and N. Lacaille, "Analysis and design of OFDM/OQAM systems based on filterbank theory," IEEE transactions on signal processing, vol. 50, no. 5, pp. 1170–1183, 2002.

[3] P. Banelli, S. Buzzi, G. Colavolpe, A. Modenini, F. Rusek, and A. Ugolini, "Modulation formats and waveforms for 5G networks: Who will be the heir of OFDM?: An overview of alternative modulation schemes for improved spectral efficiency," IEEE Signal Processing Magazine, vol. 31, no. 6, pp. 80–93, 2014.

[4] H. Bölcskei, "Orthogonal frequency division multiplexing based on offset QAM," in Advances in Gabor analysis. Springer, 2003, pp. 321–352.

[5] R. Zakaria and D. Le Ruyet, "A novel filter-bank multicarrier scheme to mitigate the intrinsic interference: Application to MIMO systems," IEEE Transactions on Wireless Communications, vol. 11, no. 3, pp. 1112–1123, 2012.

[6] R. Nissel and M. Rupp, "Pruned DFT-Spread FBMC: Low PAPR, low latency, high spectral efficiency," IEEE Transactions on Communications, vol. 66, no. 10, pp. 4811–4825, 2018.

[7] R. P. Junior, C. A. F. d. Rocha, B. S. Chang, and D. Le Ruyet, "A novel DFT precoded filter bank system with iterative equalization," IEEE Wireless Communications Letters, vol. 10, no. 3, pp. 478–482, 2021.

[8] D. Demmer, R. Zakaria, R. Gerzaguet, J.-B. Doré, and D. Le Ruyet, "Study of OFDM precoded filter-bank waveforms," IEEE Transactions on Wireless Communications, vol. 18, no. 6, pp. 2889–2902, 2018.

[9] R. P. Junior, C. A. da Rocha, B. S. Chang, and D. Le Ruyet, "A generalized DFT precoded filter bank system," IEEE Wireless Communications Letters, vol. 11, no. 6, pp. 1176–1180, 2022.

[10] R. Pereira, C. A. Da Rocha, B. S. Chang, and D. Le Ruyet, "A two-dimensional FFT precoded filter bank scheme," IEEE Transactions on Wireless Communications, 2023.

[11] R. Hadani and A. Monk, "OTFS: A new generation of modulation addressing the challenges of 5G," arXiv preprint arXiv:1802.02623, 2018.

[12] K. Murali and A. Chockalingam, "On OTFS modulation for high-doppler fading channels," in 2018 Information Theory and Applications Workshop (ITA). IEEE, 2018, pp. 1–10.

[13] C. Lélé, P. Siohan, and R. Legouable, "The alamouti scheme with CDMA-OFDM/OQAM," EURASIP Journal on Advances in Signal Processing, vol. 2010, pp. 1–13, 2010.

[14] H. G. Feichtinger and T. Strohmer, Gabor analysis and algorithms: Theory and applications. Springer Science & Business Media, 2012.

[15] R. Nissel, F. Ademaj, and M. Rupp, "Doubly-selective channel estimation in FBMC-OQAM and OFDM systems," in 2018 IEEE 88th Vehicular Technology Conference (VTC-Fall). IEEE, 2018, pp. 1–5.

[16] R. Van Nee, A. Van Zelst, and G. Awater, "Maximum likelihood decoding in a space division multiplexing system," in VTC2000-Spring. 2000 IEEE 51st Vehicular Technology Conference Proceedings (Cat. No. 00CH37026), vol. 1. IEEE, 2000, pp. 6–10.

[17] N. Benvenuto, S. Tomasin, and L. Tomba, "Equalization methods in ofdm and fmt systems for broadband wireless communications," IEEE Transactions on Communications, vol. 50, no. 9, pp. 1413–1418, 2002.

[18] R. P. Junior, C. A. F. da Rocha, B. S. Chang, and D. Le Ruyet, "Iterative interference cancellation for the DFT precoded filter bank system," in 2021 17th International Symposium on Wireless Communication Systems (ISWCS). IEEE, 2021, pp. 1–6.

[19] N. Benvenuto and S. Tomasin, "Iterative design and detection of a DFE in the frequency domain," IEEE Transactions on Communications, vol. 53, no. 11, pp. 1867–1875, 2005.

[20] S. Wu, L. Kuang, Z. Ni, J. Lu, D. Huang, and Q. Guo, "Low-complexity iterative detection for large-scale multiuser MIMO-OFDM systems using approximate message passing," IEEE Journal of Selected Topics in Signal Processing, vol. 8, no. 5, pp. 902–915, 2014.

[21] D. Bandeira, D. Le Ruyet, M. Pischella, and J. Mota, "Performance evaluation of low-complexity algorithms for orthogonal time-frequency space modulation," Journal of Communication and Information Systems, vol. 35, no. 1, pp. 138–149, 2020.

[22] E. U. T. R. Access, "Base station (BS) radio transmission and reception," 3GPP TS, vol. 36, p. V9, 2009.

[23] R. Haas and J.-C. Belfiore, "A time-frequency well-localized pulse for multiple carrier transmission," Wireless personal communications, vol. 5, no. 1, pp. 1–18, 1997.

ROGÉRIO PEREIRA JUNIOR was born in São José, Santa Catarina, Brazil, in 1994. He holds a degree in Telecommunications Systems from the Federal Institute of Santa Catarina (IFSC), Brazil in 2016, and he received his M.Sc. and D.Sc degree in electrical engineering from the Federal University of Santa Catarina (UFSC), Florianópolis, Brazil, in 2018 and 2022 respectively. He is currently an Professor of Technical and Technological Education at the IFSC, São José, Brazil. His research interests lie in the areas of digital communications and signal processing including, widely linear processing, equalization and multi-carrier systems.

CARLOS AURÉLIO FARIA DA ROCHA received his B.Sc degree in Electronic Engineering from the Federal University of Pará (UFPA), Pará, Brazil, in 1981, the M.Sc. degree in Electrical Engineering from the Federal University of Santa Catarina (UFSC), Santa Catarina, Brazil, in 1986, and the D.Sc. degree from the State University of Campinas (UNICAMP), São Paulo, Brazil, in 1996. From 1993 to 1994, he was with Laboratoire des Signaux et Systèmes, SUPELEC, Gif-Sur-Yvette, France. From 2008 to 2009, he was with the Conservatoire National des Arts et Métiers, Laboratoire Cedric Traitement du Signal et Architectures Électroniques, Paris, France. Since 1983, he has been with the Electrical Engineering Department, UFSC, where he is currently a Full Professor. His current research interests include multi-carrier communication and widely linear signal processing.

BRUNO S. CHANG was born in Curitiba, Paraná, Brazil, in 1984. He received the B.Sc. Degree in Telecommunications Engineering from the Regional University of Blumenau (FURB), Brazil, in 2006, the M.Sc. degree in electrical engineering from the Federal University of Santa Catarina (UFSC), Florianópolis, Brazil, in 2008, and the D.Sc. degree in electrical engineering from the Federal University of Santa Catarina (UFSC), Florianópolis, Brazil, and the Conservatoire National des Arts et Métiers (CNAM), Paris, France in 2012. He was a visiting professor at CNAM in 2018. He is currently an Associate Professor at the Federal University of Technology - Paraná (UTFPR), Curitiba, Brazil. His research interests lie in the areas of digital communications and signal processing, including multi-carrier systems, detection and estimation algorithms, widely linear processing and energy efficient communications.

DIDIER LE RUYET received his Eng. Degree and his Ph. D. degree from Conservatoire National des Arts et Métiers (CNAM) in 1994 and 2001 respectively. In 2009, he received the "Habilitation à diriger des recherches" from Paris XIII University. From 1988 to 1996 he was a Senior Member of the Technical Staff at SAGEM Defence and Telecommunication, France. He joined Signal and Systems Laboratory, CNAM, Paris as a research assistant in 1996. From 2002 to 2010, he was an assistant professor with the Electronic and Communication Laboratory, CNAM Paris. Since 2010 he is full professor at CNAM in the CEDRIC research laboratory. He has published more than 200 papers in refereed journals and conference proceedings and six books/book chapters in the area of communication. He has been involved in several National and European projects dealing with multicarrier transmission techniques and multi-antenna transmission. He served as Technical Program Committee member in major IEEE conferences (ICC, GLOBECOM, VTC, ISWCS, WCNC). He was General chair for ISWCS 2012 and co-General chair for ISWCS 2014 and 2019. He served as a Co-editor of a special issue of Eurasip Journal on wireless communications and networking on recent advances in multiuser MIMO systems. His main research interests lie in the areas of digital communications and signal processing including channel coding, detection and estimation algorithms, filter bank based multi-carrier communication and multi-antenna transmission. He is senior member of IEEE.